Available online at www.sciencedirect.com
ScienceDirect
Journal of Nuclear Materials 371 (2007) 118–128
journal of nuclear materials
www.elsevier.com/locate/jnucmat

Oxidation of 9Cr oxide dispersion strengthened steel exposed in supercritical water

Yun Chen [a,*], Kumar Sridharan [a], Shigeharu Ukai [b], Todd R. Allen [a]

[a] Department of Engineering Physics, University of Wisconsin, 3335 Engineering Hall, 1415 Engineering Drive, Madison, WI 53706, United States
[b] Division of Materials Science and Engineering, Hokkaido University, Japan

Abstract

The oxidation behavior of a 9 at.% Cr oxide dispersion strengthened (ODS) ferritic/martensitic (F/M) steel exposed to supercritical water at different application temperatures was examined. For comparison, two non-ODS F/M steels HCM12A (~12 at.% Cr) and NF616 (~9 at.% Cr) were also examined. The oxidized samples were characterized using gravimetry, scanning electron microscopy/energy dispersive X-ray spectroscopy, X-ray diffraction, electron back-scatter diffraction and transmission electron microscopy/selected area diffraction. A lower weight gain was consistently observed in 9Cr ODS steel at 500 °C and 600 °C. During exposure, the formation of an internal oxidation layer in the 9Cr ODS steel played a key role in establishing the oxidation behavior. In the 600 °C exposure, grain boundary diffusion of cations may no longer proceed dominantly as it did in the 500 °C exposure. Volume diffusion was likely accelerated and the bulk grains became a more important path for element migration, and the benefit from a small quantity of yttrium (0.28 wt%) in the steel became limited. However, because of the fine grain size of the 9Cr ODS steel, Cr quickly segregated to the ferritic grain boundary region in the internal oxidation layer and especially to the internal oxidation layer/base steel interface, resulting in the formation of Cr-enriched spinel ribbons and a Cr-enriched continuous spinel layer. The microstructure that developed slows down the further diffusion of both cations and anions at 600 °C.

1. Introduction

Corrosion resistance is one of the key requirements for structural materials to be used in the proposed supercritical water-cooled nuclear reactors [1]. Operating the water coolant in the supercritical state increases the operating temperature and subsequently improves the energy conversion efficiency and fuel usage, and reduces pollutant emissions [2]. The challenge to using supercritical water is that the oxidation rates are significantly enhanced beyond those seen in temperatures and pressures typically existing in water-cooled reactors [3,4].

As candidate structural material for advanced nuclear energy systems, ferritic/martensitic (F/M) steels with body center cubic structure provide good swelling resistance, low thermal expansion coefficients, and high thermal conductivity. However, their application is limited to temperatures of up to ~600 °C due to the loss of creep strength at higher temperatures. One approach to improve

* Corresponding author. Fax: +1 608 263 7451.
E-mail address: chen2@wisc.edu (Y. Chen).

0022-3115/$ - see front matter © 2007 Elsevier B.V. All rights reserved.
doi:10.1016/j.jnucmat.2007.05.018

creep characteristics at higher temperatures is strengthening by the addition of a fine dispersion of oxide particles in the matrix of the steel. Oxide dispersion strengthened (ODS) steels produced by mechanically alloying with Y_2O_3 dispersion particles have been shown to have higher creep strength compared to traditional F/M steels of similar compositions [5–8]. However, the oxidation behavior of 9Cr ODS steels in high temperature environments, such as supercritical water environment, requires investigation.

The purpose of this study was to investigate the oxidation behavior of a typical 9Cr ODS F/M steel in supercritical water at the different application temperatures being considered. The beneficial effect of yttrium, introduced as a dispersed oxide, on oxidation behavior at different temperatures was examined. For comparison, two advanced non-ODS F/M steels HCM12A (~12 at.% Cr) and NF616 (~9 at.% Cr) were also examined and studied.

2. Experimental details

Bar stock of 9Cr ODS F/M steel (24 mm diameter and 60 mm length) was supplied for this study by the Japan Atomic Energy Agency. The alloy had been annealed at 1050 °C for 60 min, air-cooled, and subsequently tempered at 800 °C for 60 min. The chemical composition of the steel is shown in Table 1. The details of the manufacturing process are described elsewhere [9]. The mean grain size of the tested 9Cr ODS steel was ~500 nm reported in a paper [10]. Two non-ODS F/M steels NF616 and HCM12A were also tested for comparison. Their chemical compositions are also shown in Table 1. The NF616 steel was normalized at 1070 °C for 2 h followed by air-cooling and tempered at 770 °C for 2 h followed by air-cooling. The HCM12A steel was normalized at 1070 °C for 1 h followed by air-cooling and tempered at 770 °C for 7 h followed by air-cooling. The typical mean grain size for both NF616 and HCM12A steels was ~10–20 μm [10].

The as received steels were cut into test samples with dimensions of 31.8 mm × 12.7 mm × 0.5 mm, polished progressively with finer grit silicon-carbide paper, and then final polished with a 1 μm diamond paste. The corrosion experiments were performed in a natural circulation supercritical water corrosion loop at 360 °C, 500 °C, and 600 °C and 25 MPa with a dissolved oxygen concentration of 20–25 ppb. The detailed construction and system capabilities of this supercritical water loop have been described in a previous paper [11]. The exposure times were 333, 690, 1026 h for the 500 °C test and 333, 667, 1000 h for the 360 °C and 600 °C tests.

After exposure, the extent of oxidation was evaluated by weight change measurement using a Scientech SA-80 Milligram Balance with an accuracy of 0.1 mg. A LEO 1530 field emission scanning electron microscope (FESEM) equipped with energy dispersive spectroscopy (EDS) was used to examine oxide structure in both plan and cross-sectional views as well as to analyze composition across the oxide layer thickness. Electron back-scatter diffraction (EBSD) analysis was performed also in the LEO 1530 FESEM incorporated with TSL orientation imaging microscopy (OIM) system. To obtain geometric exposure of internal oxidation layer, the oxidized sample was mounted on a tripod and carefully polished to remove the base alloy. The observation plane is at a depth of 70–75 μm from the gas/scale interface. Transmission electron microscopy (TEM) cross-section samples of the oxidized regions were prepared by mechanical thinning, followed by argon ion milling to achieve electron transparency. A liquid-nitrogen cooled stage, a low ion-milling current/voltage, and a low sputtering angle were used to keep the sample cool during thinning, to minimize specimen damage. Electron diffraction and diffraction-contrast imaging were conducted in a CM200 TEM operated at 200 kV.

3. Results and discussion

3.1. Oxidation kinetics

Fig. 1 shows the weight gain data of the 9Cr ODS steel after exposure to supercritical water at 500 °C and 600 °C and subcritical water at 360 °C for

Table 1
Chemical compositions of 9Cr ODS steel, NF616 and HCM12A F/M steels (wt%, Bal. Fe)

Alloy	C	Al	Si	P	S	V	Cr	Mn	Ni	Nb	Mo	W	Others
HCM12A	.11	.001	.27	.016	.002	.19	10.83	.64	.39	.054	.3	1.89	N: .063; Cu: 1.02; B: 31 ppm
NF616	.109	.005	.102	.012	.003	.194	8.82	.45	.174	.064	.468	1.87	O: .0042
9Cr ODS	.14	–	.048	<.05	.003	–	8.6	.05	.06	–	–	2	Ti: .21; Y: .28; O: .14

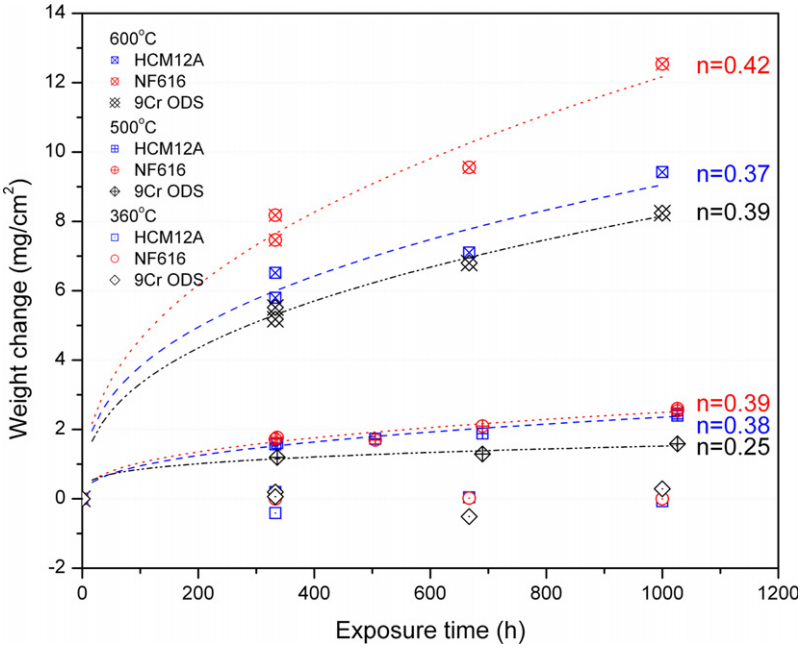

Fig. 1. Weight change as a function of exposure time obtained for F/M steels 9Cr ODS, HCM12A and NF616 in 500 °C and 600 °C supercritical water and 360 °C subcritical water environments.

different times. For comparison, the weight gain data for HCM12A and NF616 steels after similar exposures are presented in Fig. 1. For all three steels the weight gain accelerates with increasing temperature.

For the steels exposed to 500 °C and 600 °C supercritical water, the limited weight gain data shown in Fig. 1 indicates that the oxidation is temperature dependent and reasonably predictable for all steels tested. The time exponents n obtained by fitting the weight gain data using the following generalized equation:

$$\Delta W = k_p t^n, \tag{1}$$

which is usually employed to evaluate high temperature oxidation kinetics, are also summarized in Fig. 1. In Eq. (1), ΔW is weight change of the steel (mg/cm^2), k_p is rate constant, and t is exposure time (h). The weight gain data indicate that the oxidation rates of all steels follow the power laws and are in between cubic and parabolic growth behaviors. All samples exhibited a continuous protective oxide film on the steel surface. Among the tested steels, the lowest weight gain was consistently observed in 9Cr ODS steel, even though the 9Cr ODS steel has less bulk Cr than the HCM12A.

At 600 °C, the oxidation behavior of the 9Cr ODS is close to that of the higher Cr F/M steel HCM12A, while its oxidation behavior shows a remarkable improvement at 500 °C even compared with that of 12 at.% Cr HCM12A. In 360 °C subcritical water, for these short-term exposures, all three steels exhibit low, but fluctuating weight changes.

The weight gain as a function of scale thickness for the three steels is presented in Fig. 2. The non-ODS steels, HCM12A and NF616, steadily gain oxygen. The linear proportionalities between weight gain and thickness for the HCM12A and NF616 steels indicate that the density of the scale is relatively constant. However, the 9Cr ODS steel shows a weight gain that is not proportional to the film thickness, especially for samples exposed to 500 °C supercritical water, indicating that the scale density decreases gradually. With increasing exposure time the scale structure tends to become more porous.

Such oxidation behavior could be explained by the grain boundary diffusion associated with oxidation temperature. According to the classification of diffusion kinetics by Harrison [12,13], in the limiting case of high temperatures, and/or very long anneals (exposure), and/or small grain sizes, the effective diffusion coefficient D_{eff} can be represented by an average of volume diffusion coefficient D and grain boundary diffusion coefficient D_b weighted by the

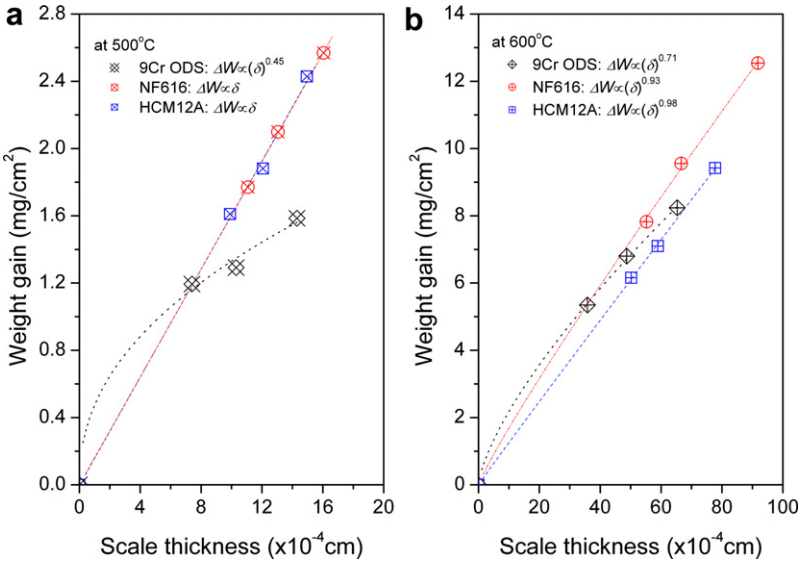

Fig. 2. Weight change (ΔW) as a function of scale thickness (δ) for the tested steels exposed to supercritical water at (a) 500 °C and (b) 600 °C.

ratio of the number of diffusing atoms in the grain boundaries to that in the grain [12]:

$$D_{\text{eff}} = fD_{\text{b}} + (1-f)D, \tag{2}$$

where f is the volume fraction of grain boundaries in the polycrystal, i.e. $f = q\delta/d$, q being a numerical factor depending on the grain sharp, ($q = 1$ for parallel grain boundaries), δ being grain boundary thickness, and d being spacing between grain boundaries (grain size) in a polycrystalline material. If there is grain boundary segregation of the diffusing atoms, then $f = qs\delta/d$, where s is segregation factor.

Grain boundary effects in polycrystalline silver became measurable only below 750 °C and they became relatively more important as the temperature was decreased [14,12]. This is a general effect and indicates that the activation energy for grain boundary diffusion is appreciably less than that for lattice diffusion, and the effect could be especially enhanced in the 9Cr ODS steel due to grain boundary yttrium segregation.

In our previous work [15], we discussed the decrease in density and suggested that a small quantity of yttrium preferentially segregated to oxide ribbons that formed along the grain boundary regions in the internal oxidation layer. The formation of these ribbons reduced the cation outward flux at these regions, while not significantly affecting inward oxygen diffusion. The depletion of iron cations in the $(FeCr)_3O_4$ layer resulted in the formation of vacancies which eventually coalesce into pores and thereby caused the gradual decrease of the scale density with the increase of the exposure time. On the other hand, for higher temperature exposure, a mitigation of such density decrease is observed in Fig. 2(b). Increasing the temperature not only resulted in the increase of diffusivities for all species; but also decreases the contribution of diffusion along grain boundaries and dislocations (for a given dislocation density) [14]. At 600 °C, in our case, the diffusion of iron cations may no longer proceed dominantly along the boundary regions as it did in the 500 °C exposure. The diffusion through crystals was likely accelerated and the bulk grains became a more important path for element migration. The benefit from a small quantity of yttrium (0.28 wt%) in the steel became limited.

3.2. Oxide microstructure and compositions

Fig. 3 shows the surface morphologies of the oxide scales formed on the F/M steel 9Cr ODS after exposure to supercritical water at 500 °C and 600 °C and subcritical water at 360 °C. The influence of test temperature on the outer layer grain size is significant. At 500 °C, the outer grain sizes are approximately 2–5 μm for 336 h exposure. Exposure at 600 °C supercritical water leads to faster growth of the outer grains, which have grain sizes in the range

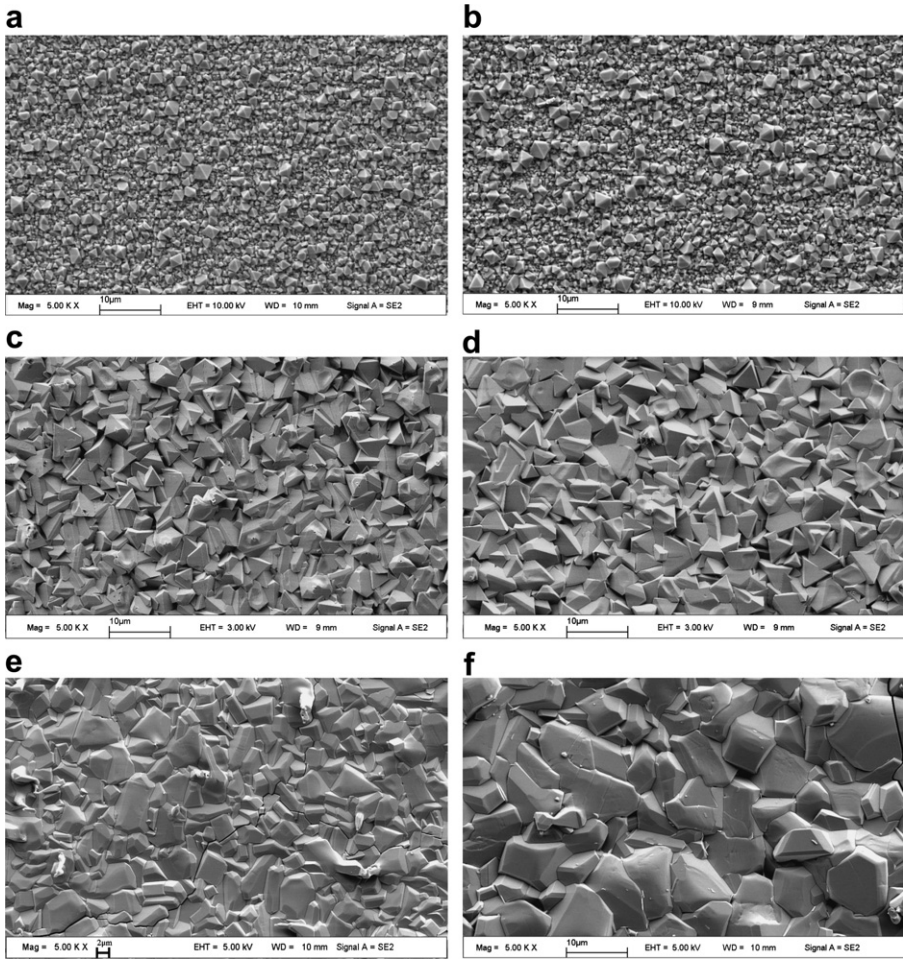

Fig. 3. SEM images showing the surface morphologies of the scales formed on F/M steel 9Cr ODS after exposure to subcritical water at 360 °C and supercritical water at 500 °C and 600 °C for 333 h and 1000 h, respectively (a) at 360 °C for 333 h, (b) at 360 °C for 1000 h, (c) at 500 °C for 336 h, (d) at 500 °C for 1026 h, (e) at 600 °C for 333 h and (f) at 600 °C for 1000 h.

of 2–8 μm for 333 h exposure and typically became larger than 10 μm after 1000 h exposure.

At 360 °C, on the other hand, most oxide grains are approximately 1 μm in size for the 333 h exposure, and the size shows a slight increase when the exposure time was increased to 1000 h. The X-ray diffraction patterns in Fig. 4 show that those oxide gains are mainly of a spinel compound.

The intensity of the diffraction peaks corresponding to ferrite phase are strong, suggesting that the scale developed at 360 °C was very thin even for exposure times to 1000 h. The corrosion rate of the tested steels in the 360 °C subcritical water environment is relatively slow with little oxide formed in the duration of these tests. When temperature is below the critical point of water ($T_c = 374$ °C, $P_c = 22.1$ MPa), the density, dielectric constant, and ionic product of water significantly increase [16]. Such changes could result in the increased mechanical removal of surface oxides by water or increased solubility of reaction products in water. The possible influence of water density on the adhesion of the surface oxide grains is also supported by the weight gain results as seen in Fig. 1 where 360 °C exposed steel exhibited a slight loss in weight.

The morphology and atomic composition vs. depth profiles taken on the oxidized 9Cr ODS cross-sections using EDS are shown in Fig. 5. Fig. 5 indicates that several layers, including an outer Fe_3O_4 magnetite layer, an inner $(FeCr)_3O_4$ layer and an innermost internal oxidation layer, were formed on 600 °C exposed 9Cr ODS steel. This structure is similar to those scales developed in

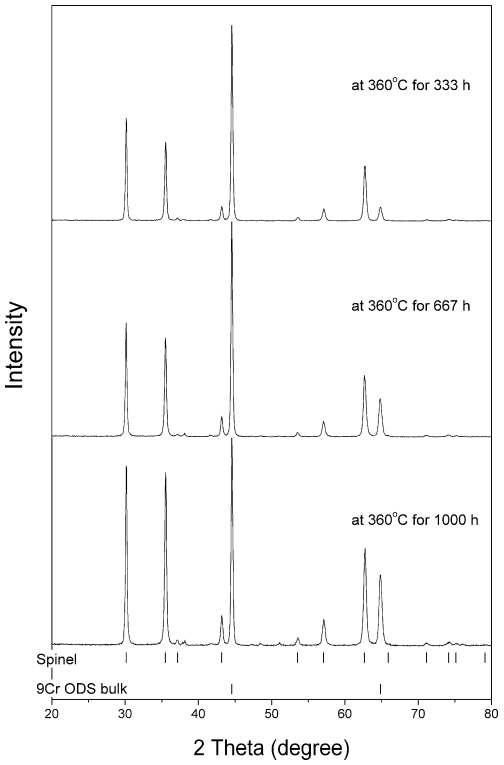

Fig. 4. X-ray patterns obtained from the surface of the 9Cr ODS steels after exposure to 360 °C subcritical water for 333 h, 667 h and 1000 h.

500 °C exposure test samples [15]. Unique to the samples exposed at 600 °C is a ~1 μm thick, dense and continuous Cr-rich oxide layer developed along the interface between internal oxidation layer and base metal.

The internal oxidation layer in the 9Cr ODS steel after exposure for 1000 h at 600 °C is thinner than that in the 667 h exposed sample, while the outer Fe_3O_4 magnetite layer and inner $(FeCr)_3O_4$ spinel layer increased in thickness with increasing exposure time. Due to the significant difference of the outward diffusion rates between Fe and Cr cations [17], the interface of magnetite layer and spinel layer is commonly accepted to coincide with the original steel surface [18]. EDS results show that the depth of the spinel plus the internal oxidation layer after 667 h exposure is approximately 48 μm. This depth corresponds to the distance from the original steel surface into the metal to the maximum distance to which oxygen has penetrated. Correspondingly, this depth is only ~40 μm depth after exposure for 1000 h. The evidence implies that the depth of the spinel plus the internal oxidation layer in 9Cr ODS steel at 600 °C can rapidly reach a thickness of about 40–50 μm. Then, a 1 μm Cr-enriched oxide layer formed along the internal oxidation layer/base steel interface acts as a diffusion barrier to further inward diffusion of oxygen.

SEM images in Fig. 5 did not show any sign of spallation or even formation of cavities at the layer interfaces. The adhesion of the scale was good with no spallation even at an exposure temperature of 600 °C. A large number of small pores were dispersed in the spinel layer but this level of porosity did not lead to spallation. Several cracks in Fig. 5(a) and (b) could be observed to occur in the surface of the scale. But those cracks did not propagate deep into the scales, and thus may not significantly decrease the stability of the entire scale.

The phase distribution and the grain structure throughout the scales formed on 9Cr ODS steel after exposure to supercritical water at 500 °C and 600 °C for about 1000 h were studied using EBSD and the results are seen in Figs. 6 and 7, respectively. Both show multi-layered oxide scales. At 500 °C, a double-layered scale was formed and composed of an outer layer of magnetite with a columnar grain structure and an inner layer of Fe–Cr oxide spinel with an equiaxed grain structure. The internal oxidation layer was identified to be ferrite phase and no clear interface can be observed to differentiate this layer from the base alloy. On the other hand, higher temperature (600 °C) exposure leads to a different microstructure for the scale and internal oxidation layer. As shown in Fig. 7, coarser magnetite grains developed in the outer magnetite layer, indicating a faster grain growth process; while the inner magnetite layer contains a relatively high grain density and slightly larger grains than those formed in the 500 °C environment. The most noticeably different feature between the 500 °C and 600 °C exposures is that a distinct $(FeCr)_3O_4$ spinel layer develops along the region between the internal oxidation layer and the base steel. The SEM image of Fig. 5(b) supports this observation. The EDS linescan result in Fig. 5(b) exhibits that this spinel layer contains much higher Cr than the spinel layer right adjacent to the magnetite layer.

3.3. Internal oxidation layer

In a previous study, it was noted that, in the 9Cr ODS steel after exposure to supercritical water at 500 °C, oxide ribbons formed along the grain boundaries in the internal oxidation layer and yttrium preferentially segregated to these ribbon

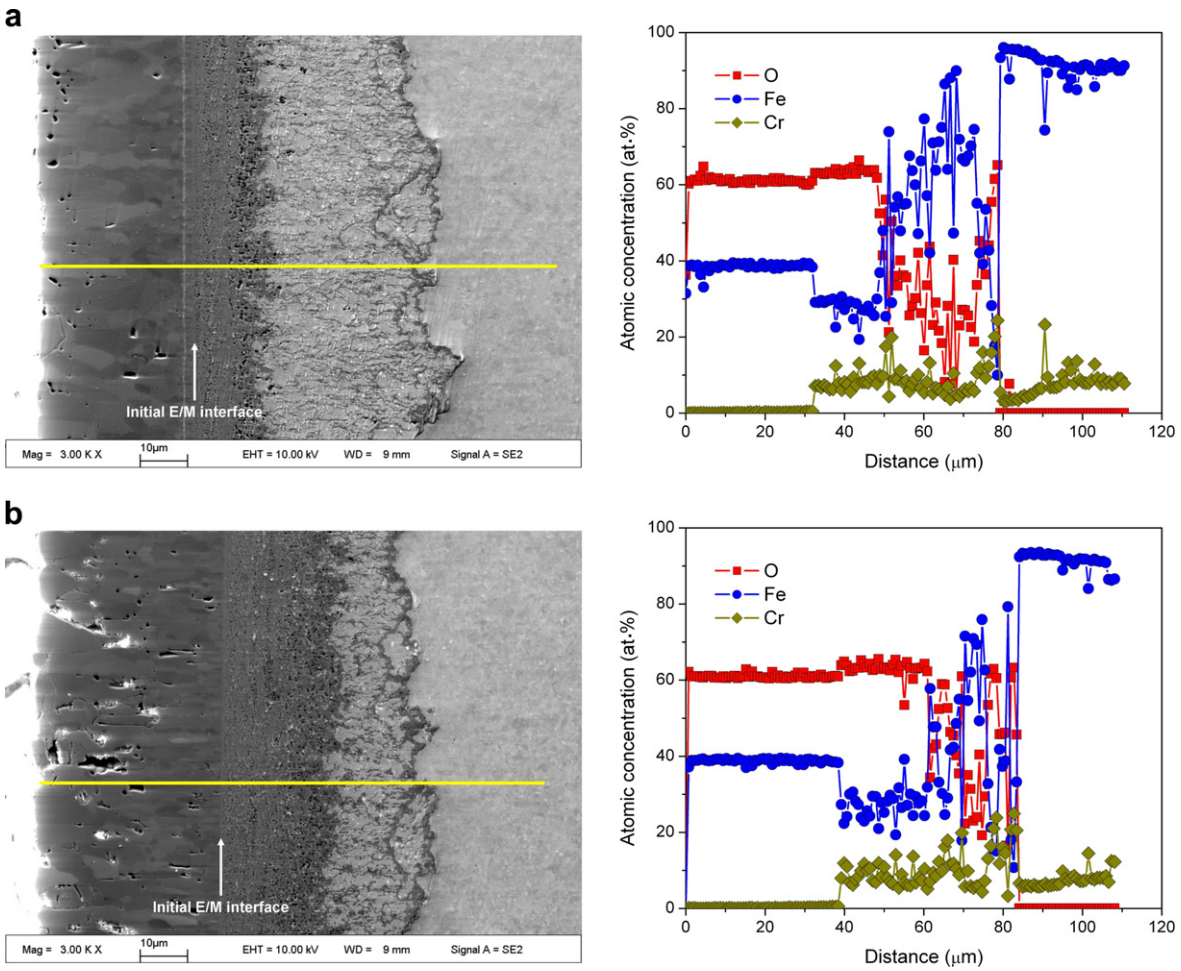

Fig. 5. SEM images showing the cross-sectional morphologies of the scale formed on 9Cr ODS samples after exposure to 600 °C supercritical water. The associated composition profiles across the scale thickness for major elements are shown. The original environment/metal (E/M) interfaces prior to exposure are indicated by the arrows in the figures Fig. 4 X-ray patterns obtained from the surface of the 9Cr ODS steels after exposure to 360 °C subcritical water for 333 h, 667 h and 1000 h (a) scale formed on 9Cr ODS steel after 667 h exposure at 600 °C and (b) scale formed on 9Cr ODS steel after 1000 h exposure at 600 °C.

regions [15]. The formation of these ribbons reduces the cation flux at these regions. Evidence for a similar mechanism was also investigated for the 600 °C exposed sample. To find the contributing factors, a series of further examinations including SEM with EDS, XRD and TEM with selected area diffraction (SAD) analysis were performed on the internal oxidation layer of the 9Cr ODS steel after exposure to 600 °C supercritical water for 1000 h. Major results are shown in Figs. 8–10 and Table 2. For comparison, a TEM micrograph showing the microstructure of the internal oxidation layer formed at 500 °C is shown in Fig. 11.

The SEM image obtained from the internal oxidation layer of the ODS steel exposed to supercritical water at 600 °C shown in Fig. 8 indicates that this internal oxidation layer is typically composed of three different regions including a dark isolated oxide region (noted by arrow 1), intergranular ribbon regions (noted by arrow 2), and the bright ODS ferritic grain region (noted by arrow 3). The chemical compositions of three regions were examined by EDS analysis and the results are summarized in Table 2. X-ray diffraction analysis was carried out and is shown in Fig. 9. Three phases were identified in this layer including two dominant phases 9Cr ODS bulk ferrite and spinel ($FeCr_2O_4$), and one minor phase eskolaite (Cr_2O_3).

The ferritic grains in this internal oxidation layer were partly oxidized. The Cr content of the intragranular area is lower than the grain boundary region because of fast segregation of Cr towards

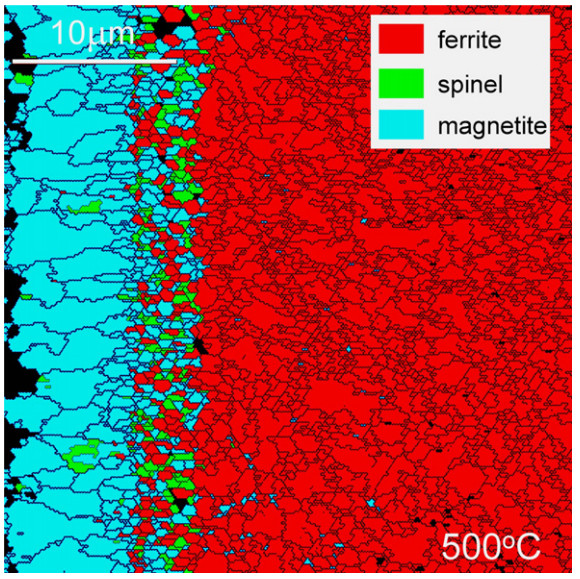

Fig. 6. Phase distribution and grain structure across the oxide scale for the 9Cr ODS steel exposed to 500 °C supercritical water for 1026 h.

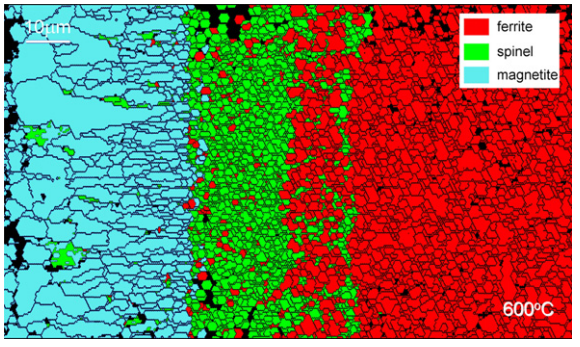

Fig. 7. Phase distribution and grain structure across the oxide scale for the 9Cr ODS steel exposed to 600 °C supercritical water for 1000 h.

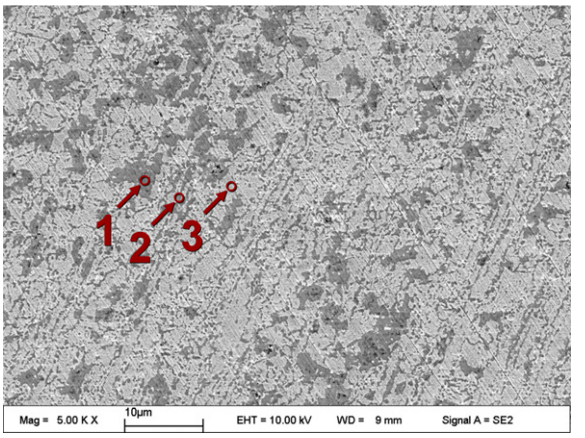

Fig. 8. Plan view of the internal oxidation region on the 9Cr ODS steel after exposure to 600 °C supercritical water for 1000 h.

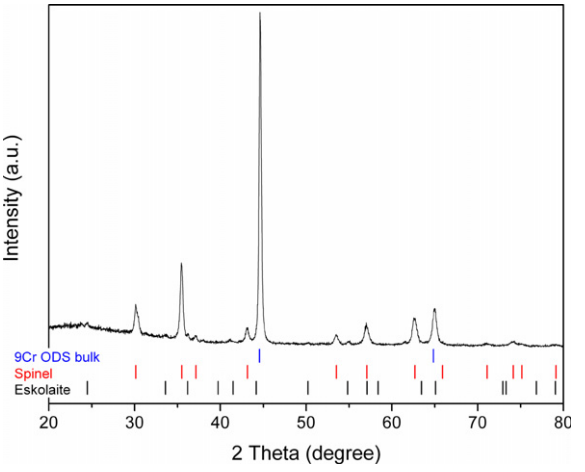

Fig. 9. XRD pattern for the internal oxidation layer of the 9Cr ODS steel after exposure to 600 °C supercritical water.

grain boundaries. Correspondingly, a Cr-enriched oxide ribbon had developed along the boundaries of ferritic grains. This observation suggests the possibility that the ribbon acts as a diffusion barrier to the inward migration of oxygen and outward migration of metallic elements along the grain boundaries. However, the ribbons are not continuous and such structure opens a possible lattice diffusion path for reaction of cations and anions.

The TEM image of Fig. 10 clearly shows the morphologies of the grains, the grain boundaries, and the oxide ribbons. The SAD pattern in the lower right corner of Fig. 10, which was taken from

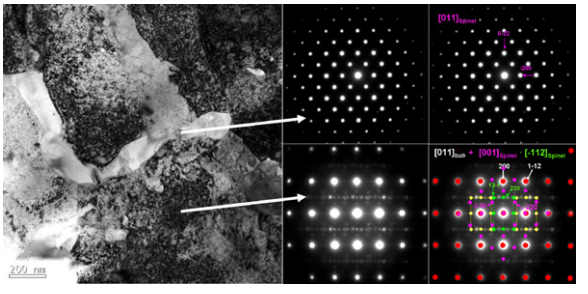

Fig. 10. TEM image with selected area diffraction patterns showing the morphology and phases of the grains and grain boundaries in the internal oxidation layer of the 9Cr ODS steel after exposure to 600 °C supercritical water for 1000 h.

Table 2
Atomic compositions of three regions as marked by arrows in Fig. 8

	O–K	Ti–K	Cr–K	Fe–K	W–M
Point 1	60.89	0.23	7.37	31.03	0.48
Point 2	64.03	0.31	13.86	21.55	0.24
Point 3	24.58	0.42	5.91	68.88	0.21

the intragranular region, reveals the grain is composed of two components including ferrite and spinel. The oxide ribbons developed only along the grain boundaries. Few defects exist in this ribbon region. The SAD pattern taken from the ribbon region in right upper corner of Fig. 10 illustrates these oxide ribbons are essentially spinel and are free of secondary phases. By comparing Fig. 10 for the 600 °C exposed sample with Fig. 11 for 500 °C sample, we conclude that both formed a similar microstructure in the internal oxidation layer. The only obvious difference is that in the 600 °C sample, a much wider oxide ribbon region (~100–200 nm) was formed. Such structure is consistent with the SEM observation in Fig. 8.

Based on the above results and discussion, it seems there is not a significant difference between the basic components of the internal oxidation layer formed at 500 °C and 600 °C. However, as shown in Section 3.1, the oxidation behavior of the 9Cr ODS at 600 °C, especially the change of scale density with exposure time, is different compared with the samples in 500 °C exposure. Our understanding is the oxide ribbon in the internal oxidation layer may no longer dominantly influence the oxidation behavior as it did at 500 °C. It is likely other contributing factors play a role in establishing the oxidation behavior at 600 °C.

Increasing Cr content is known to promote the formation a more continuous protective scale, and thereby increase the oxidation resistance of an high-chromium F/M steel [19–21]. Reducing grain size of a Fe–Cr steel has been recognized to be another effective approach to improve its oxidation resistance because fine grain size allows rapid segregation of Cr to the grain boundary and surface, where it can react with oxygen to form the Cr rich oxide scale [14,19,22]. In our case, we discussed in Section 3.1 that the benefit from a small quantity of yttrium was limited at higher temperature. However, owing to the fine grain size of the 9Cr ODS steel (~500 nm), the Cr-enriched spinel ribbons

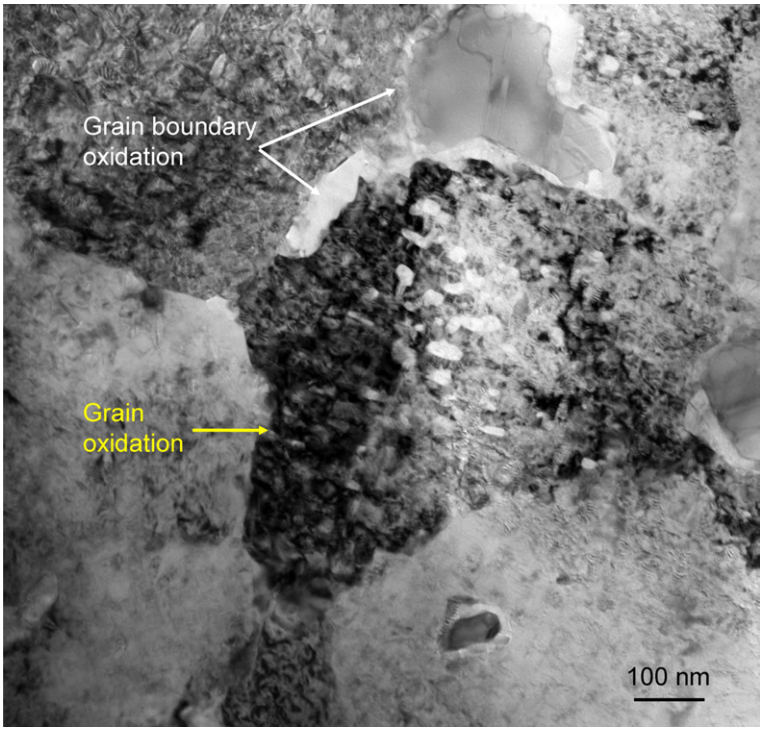

Fig. 11. TEM image showing the morphology of the grains and grain boundaries in the internal oxidation layer of the 9Cr ODS steel after exposure to 500 °C supercritical water for 1026 h.

along the ferritic grain boundaries in the internal oxidation layer and especially the Cr-enriched spinel layer along the interface between the internal oxidation layer and the base steel quickly formed. And the microstructure thus developed slows down the further diffusion of both cations and anions. As a result, the 9Cr ODS steel again shows a much better oxidation resistance in a higher temperature supercritical water (600 °C) even compared with the higher Cr content F/M steel HCM12A.

4. Conclusion

The oxidation rate of 9Cr ODS steel at exposure temperatures of 500 °C and 600 °C follows a power law with kinetics between cubic and parabolic rates. 9Cr ODS steel consistently shows the lower weight gain compared to NF616 and HCM12A, even though the 9Cr ODS steel has less bulk Cr than the HCM12A.

At 600 °C, grain boundary diffusion of cations may no longer proceed dominantly as it did at 500 °C. Volume diffusion was likely accelerated and the bulk grains became a more important path for element migration. The benefit from a small quantity of yttrium (0.28 wt%) in the steel became limited at higher temperature.

Owing to the fine grain size of the 9Cr ODS steel, the Cr-enriched spinel ribbons along the ferritic grain boundaries in the internal oxidation layer and the Cr-enriched continuous spinel layer along the internal oxidation layer/base steel interface quickly formed. The microstructure that developed slows down the further diffusion of both cations and anions at 600 °C as compared to traditional F/M steels.

Disclaimer

'This report was prepared as an account of work sponsored by an agency of the United States Government. Neither the United States Government nor any agency thereof, nor any of their employees, makes any warranty, express or implied, or assumes any legal liability of responsibility for the accuracy, completeness, or usefulness of any information, apparatus, product, or process disclosed, or represents that its use would not infringe privately owned rights. Reference herein to any specific commercial product, process, or service by trade name, trademark, manufacturer, or otherwise does not necessarily constitute or imply its endorsement, recommendation, or favoring by the United States Government or any agency thereof. The views and opinions of authors expressed herein do not necessarily state or reflect those of the United States Government or any agency thereof'.

Acknowledgements

The work is supported by the Idaho National Laboratory as part of the Department of Energy Generation IV Initiative and by the Department of Energy Office of Nuclear Energy, Science, and Technology NERI program (project 05-151) under contract DE-FC07-05ID14664. The authors thank the following University of Wisconsin personnel who contributed to the testing of the samples reported in this work: X. Ren, L. Tan, M. Anderson, J. Licht, A. Kruizenga.

References

[1] T.R. Allen, D.C. Crawford (Eds.), Proceedings of the ICAPP'03, American Nuclear Society, Cordoba, Spain, 2003, paper 3237.
[2] K.H. Mayer, in: International Joint Power Generation Conference, PWR-Vol. 33, ASME, 1998, p. 831.
[3] R. Viswanathan, in: Proceedings of the 2000, International Joint Power Generation Conference, Miami Beach, FL 2000, p. 1.
[4] M. Bethmont, Mater. High Temp. 15 (1998) 231.
[5] T. Allen, R.L. Klueh, S. Ukai, in: Fuels and Materials for Transmutation, OECD NEA Report Number 5419, 2005, 135.
[6] S. Ohtuska, S. Ukai, M. Fujiwara, T. Kaito, T. Narita, Mater. Trans. 46 (3) (2005) 1.
[7] S. Ukai, S. Mizuta, T. Yoshitake, T. Okuda, M. Fujiwara, S. Hagi, T. Kobayashi, J. Nucl. Mater. 283–287 (2000) 702.
[8] M.K. Miller, D.T. Hoelzer, E.A. Kenik, K.F. Russell, Intermetallics 13 (2005) 387.
[9] S. Ohtuska, S. Ukai, M. Fujiwara, T. Kaito, T. Narita, Mater. Trans. 46 (3) (2005) 1.
[10] Yun Chen, Kumar Sridharan, Todd R. Allen, in preparation.
[11] K. Sridharan, A. Zillmer, J.R. Licht, T.R. Allen, M.H. Anderson, L. Tan , in: Proceedings of ICAPP04, Pittsburgh, PA, 2004, p. 537.
[12] Y. Mishin, Chr. Herzig, J. Bernardini, W. Gust, Int. Mater. Rev. 42 (4) (1997) 155.
[13] L.G. Harrison, Trans. Faraday Soc. 57 (1961) 1191.
[14] P. Shewmon, Diffusion in Solid, McGraw-Hill, New York, 1963.
[15] Y. Chen, K. Sridharan, T.R. Allen, S. Ukai, J. Nucl. Mater. 359 (2006) 50.
[16] P. Kritzer, J. Supercrit. Fluids 29 (2004) 1.
[17] J. Robertson, Corros. Sci. 32 (4) (1991) 443.
[18] J. Zhang, N. Li, Oxid. Met. 63 (2005) 353.
[19] R.L. Klueh, D.R. Harries, ASTM Stock Number: MONO3, West Conshohocken, 2001.

[20] A. Fleming, R.V. Maskell, L.W. Buchanan, T. Wilson, in: A. Strong (Ed.), Materials for High Power Generation and Process Plant Applications – Book 728, The Institute of Materials, London, 2000, p. 33.
[21] P.J. Ennis, W.J. Quadakkers, in: A. Strang, W.M. Banks, R.D. Conroy, G.M. McColvin, J.C. Neal, S. Simpson (Eds.), PARSONS 2000, Advanced Materials for 21st Century Turbines and Power Plant – Book 736, The Institute of Materials, London, 2000, p. 265.
[22] S.N. Basu, G.J. Yurek, Oxid. Met. 36 (1991) 281.